

**Linear and nonlinear edge and corner states in graphenelike moiré lattices**

Chengzhen Lu, Yuanmei Gao, Xuefei Cao, Yingying Ren,<sup>\*</sup> Zhanghua Han<sup>Ⓞ</sup>, Yangjian Cai, and Zengrun Wen<sup>Ⓞ†</sup>  
*Shandong Provincial Engineering and Technical Center of Light Manipulation & Shandong Provincial Key Laboratory of Optics  
 and Photonic Devices, School of Physics and Electronics, Shandong Normal University, Jinan 250358, China  
 and Collaborative Innovation Center of Light Manipulation and Applications, Shandong Normal University, Jinan 250358, China*



(Received 26 May 2023; revised 16 July 2023; accepted 18 July 2023; published 26 July 2023)

Graphene structures play a fundamental role in the exploration of edge states, topological insulators, and electronic transport applications. In this paper, we propose a graphenelike moiré photonic lattice formed by superimposing two identical triangle sublattices with an antiphase and a specific twist angle and study the edge and corner states of such a lattice in linear and nonlinear regimes. The graphenelike moiré lattice is truncated into three types of edges in analogy with those of graphene. Through band-structure calculations, we find that only the zigzag edge supports edge states, while the other two edges do not exhibit such states. A truncated graphenelike moiré photonic lattice with zigzag edges is constructed by utilizing the laser-writing technique. We observe the complex edge states and corner states in the linear regime at the zigzag edge. Furthermore, by introducing nonlinearity, the optical localization occurs at the edges and corners. Our research provides a route for exploring topological edge states and nonlinear edge solitons in coherent moiré photonic lattices and brings possibilities for subsequent technological development in electronic or optoelectronic devices.

DOI: [10.1103/PhysRevB.108.014310](https://doi.org/10.1103/PhysRevB.108.014310)

**I. INTRODUCTION**

Photonic lattices are waveguide arrays that are realized through artificially designed refractive index modulation. Owing to the mathematical similarity between the paraxial wave equation of photonic lattices and the Schrödinger equation for the evolution of the wave function in the quantum systems, the spatial evolution of light in photonic lattices is analogous to the temporal evolution of wave function in quantum systems [1,2]. Photonic lattices can be utilized to explore physical phenomena that are difficult to achieve or directly observe in condensed physics and quantum systems [3–5]. Among the various physical phenomena, optical localization is a significant research topic that holds great potential for optical manipulation and transmission in photonic integrated devices. In the past few decades, several techniques have been employed to achieve optical localization in photonic lattices. For example, introducing disorder into coupling or potentials to mitigate dispersion can lead to Anderson localization [6,7]; Bloch oscillations can be observed by applying gradient transverse or longitudinal potentials [8,9]. By carefully designing the lattice structure to induce flat bands, optical localizations can be achieved with specific excitations [10–12]. Under nonlinear conditions, the potential energy distribution of the photonic lattice will change, which will further affect the evolution of probe light and produce many physical phenomena [13–15]. Nonlinear effects can also be utilized to balance discrete diffraction and realize nonlinear localization of light beams, facilitating the formation of discrete solitons [16,17]. The aforementioned localization techniques confine energy

within the bulk of photonic lattices. There is another widely concerned optical localization that localizes the light at the edges. In addition, photonic lattice systems have been widely studied in rapidly developed topological photonics [18–20], non-Hermitic optics [21,22], and synthetic dimensions [23].

Edge states play a crucial role in the design of future electronic and optoelectronic devices by effectively controlling light propagation [24–26]. Edge states were predicted to exist at the zigzag edges of graphene lattice, where a topological phase transition with gap opening induces topological edge states by breaking time-reversal symmetry [27–30]. The advantages of edge states have spurred investigations in topological photonic lattices, including topological photonics, edge solitons, optical isolation, and bistability [31,32]. In recent years, topological edge states and topological corner states have become fascinating frontiers of research due to their robustness against disorder and their ability to manipulate light propagation [33–35]. The introduction of nonlinearity into topological edge states leads to the formation of topological edge solitons, which can travel along the edges while maintaining localized shapes without broadening [36,37].

Moiré lattices, formed by the coherent superposition of two or more mutually twisted periodic structures, have emerged as a thriving research area in physics. Initially, moiré lattices exhibited profound physical effects in condensed matter physics, particularly in twisted graphene bilayers [38–42]. They have been associated with the discovery of unconventional superconductivity and ferroelectricity [43,44], the quantum Hall effect [45], and edge transport phenomena [46,47]. Moreover, moiré lattices have found applications in manipulating ultracold atoms [48,49], creating gauge potentials [50], and theoretical investigations of Bose-Einstein condensates [51]. In the photonic lattice area, the counterpart

<sup>\*</sup>ryywy@sdu.edu.cn

<sup>†</sup>wenzengrun@163.com

of moiré lattices can be constructed by coherently superimposing periodic square or hexagonal lattices in photorefractive materials based on weak light nonlinear effects. These moiré lattices enable the transition between localization and delocalization of bulk excitations by solely changing the twist angle between the sublattices [52]. When Kerr nonlinearity is taken into account, solitons have also been observed in such moiré lattices [53]. The localization properties of moiré lattices have an impact on the excitation of two-dimensional quadratic multifrequency solitons [54]. Current research focuses on the existence of linear and nonlinear light localization at the edges and corners of truncated square moiré lattices [55]. The significant role of graphene in the edge localization and specific advantage of moiré photonic lattices in optical localization indicate the importance of studying edge states in hexagonal moiré structures.

In this paper, we propose a graphenelike moiré lattice designed by superimposing two periodically rotated triangle sublattices with out of phases. By using the tight-binding approximation, we calculate the band structures of the moiré lattice with zigzag, bearded, and armchair edges. The calculations reveal that only the zigzag edge supports an edge mode. Further, the edge state and corner state in the triangle-shaped graphenelike moiré lattice with zigzag edges are studied both theoretically and experimentally. By utilizing the continuous wave (CW) laser-writing technique, we observe distinctive edge states and corner states under different excitations in both the linear and nonlinear photonic moiré lattices. In the linear regime, the edge and corner excitations are coupled into the nearest waveguides that are encompassed by edge modes, while the light energy is well localized in the excited waveguides for the nonlinear regime. These findings contribute to the understanding of topological edge states and nonlinear edge solitons in coherent moiré photonic lattices.

## II. MODEL AND PRINCIPLES

The coupled moiré lattices are composite structures composed of two identical periodic sublattices interfering in the  $x$ - $y$  plane. The general expression for the coupled moiré lattices can be written as

$$L_M = \sum_{j=0}^{N-1} A e^{i(\mathbf{k}_j \cdot \mathbf{r} + \theta + \varphi_j)} + \sum_{j'=0}^{N'-1} A e^{i(\mathbf{k}_{j'} \cdot \mathbf{r} - \theta + \varphi_{j'})}, \quad (1)$$

where  $A$  is the amplitude of light beam,  $\varphi_j$  and  $\varphi_{j'}$  represent the initial phase of two sublattices,  $N$  and  $N'$  are the number of interference beams in the sublattice light field, and  $\theta$  is twisted angle. The wave vectors of two lattices are  $\mathbf{k}_j = k_0[\cos(\frac{2j\pi}{N}), \sin(\frac{2j\pi}{N})]$  and  $\mathbf{k}_{j'} = k_0[\cos(\frac{j'2\pi}{N'}), \sin(\frac{j'2\pi}{N'})]$ , respectively, where  $k_0 = 2\pi/\lambda$  is the wave vector. The moiré lattice in this paper is constructed by antiphase superposition of two identical triangle sublattices with a twisted angle  $2\theta$ ; the corresponding expression is

$$L_M = \sum_{j=0}^2 A e^{ik_0[\cos(\frac{2j\pi}{3} + \theta)x + \sin(\frac{2j\pi}{3} + \theta)y]} + \sum_{j'=0}^2 A e^{i\pi} e^{ik_0[\cos(\frac{2j'\pi}{3} - \theta)x + \sin(\frac{2j'\pi}{3} - \theta)y]}, \quad (2)$$

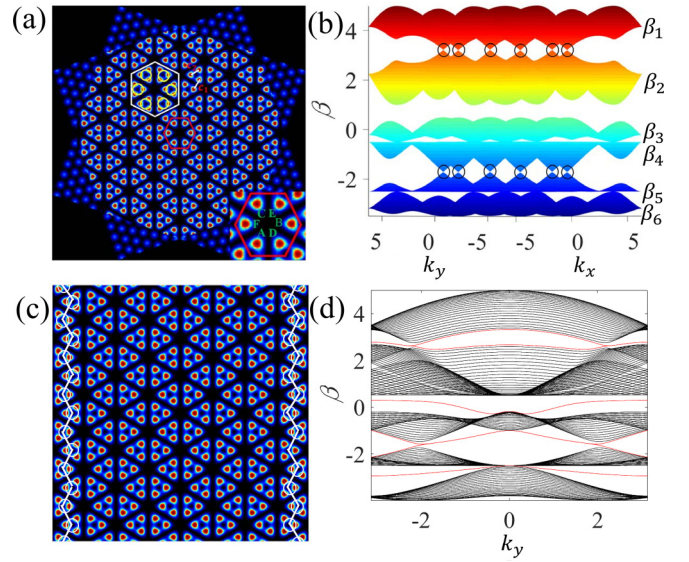


FIG. 1. Graphenelike moiré lattice structure and band structure. (a) Schematic of periodic graphenelike moiré lattice superimposed by two sublattices with the antiphase and a twist angle  $\theta = \arctan \sqrt{3}/5$ . The structure in the red regular hexagon represents a unit cell. The coupling coefficients between the intracell and intercell waveguides are  $c_1$  and  $c_2$ , respectively. (b) Band structure of the infinite graphenelike moiré lattice, the black circles signify the Dirac points. (c) Schematic image of a graphenelike moiré lattice with zigzag edge truncated on two terminations of  $x$  direction. (d) Zigzag edge band structure of graphenelike moiré lattice, red lines and black lines indicate edge states and bulk states, respectively.

where  $N = N' = 3$  and the initial phase of two sublattices are  $\varphi_j = 0$  and  $\varphi_{j'} = \pi$ . Each triangle sublattice is formed by the interference of three plane waves. The two triangular sublattices coherently superimposed with the antiphase are rotated in opposite directions, and the twist angle between them is  $\theta = \arctan \sqrt{3}/5$ . The obtained photonic lattice field is nondiffractive, and the periodicity remains as the twisted angle satisfies  $\theta = \arctan \frac{\sqrt{3}}{3}(1 - \frac{2}{C})$ ,  $C$  is a integer within a range of  $[2, +\infty)$  [56]. Figure 1(a) depicts this moiré lattice produced by two superimposed triangle sublattices. We can see that this moiré lattice has a complex hexagonal structure which is similar to the graphene photonic lattice when the three nearest components (marked by yellow circles) are considered as a whole. Therefore, we name the lattice the graphenelike moiré lattice. Each unit cell of the graphenelike moiré photonic lattice consists of six lattice sites (A–F), as marked in the red regular hexagon.

In the paraxial approximation, the propagation of the light beam in the photonic lattice is described by the Schrödinger-like equation

$$i \frac{\partial \psi(x, y, z)}{\partial z} = -\frac{1}{2k_0} \nabla^2 \psi(x, y, z) - \frac{k_0 \Delta n(x, y)}{n_0} \psi(x, y, z), \quad (3)$$

where  $\psi(x, y, z)$  is the electric field envelope of the probe beam,  $z$  is the longitudinal propagation distance that plays the role of time in the quantum mechanics Schrödinger equation,  $\nabla^2 = \partial^2/\partial x^2 + \partial^2/\partial y^2$  is the Laplacian in the transverse

plane,  $k_0 = 2n_0\pi/\lambda_0$  is the wave number within the medium, and  $n_0$  is the background refractive index of the medium.  $\Delta n$  is the linear refractive index change in a nonlinear photorefractive crystal, the photorefractive strontium barium niobite (SBN) crystal is used in our experiment. When the nonlinearity is considered, a nonlinear potential is added in Eq. (3) [15], there is

$$i\frac{\partial\psi}{\partial z} = \left[ -\frac{1}{2k_0}\nabla^2 - \frac{k_0\Delta n_L(x,y)}{n_0} - \frac{k_0\Delta n_{NL}(|\psi|^2)}{n_0} \right] \psi = (K + V_L + V_{NL})\psi, \quad (4)$$

where  $K$  is kinetic energy term,  $V_L$  is a linear potential energy term related to  $\Delta n_L(x,y)$ , and  $V_{NL}$  is a nonlinear potential energy term related to  $\Delta n_{NL}(|\psi|^2)$ . The refractive index variation can be written as  $\Delta n(x,y) = \Delta n_L(x,y) + \Delta n_{NL}(|\psi|^2)$ . Correspondingly, in the SBN crystal, the refractive index change is written as  $\Delta n(x,y) = -\frac{1}{2}n_0^3\gamma_{33}E_0\frac{1}{1+I_L+I_P}$  [15]. The parameters corresponding to the experiment are  $\lambda_0=532$  nm,  $n_0=2.35$ ,  $\gamma_{33}$  is the electro-optic coefficient ( $\gamma_{33}=280$  pm/V), and  $E_0$  is the bias field ( $E_0=1.4$  kv/cm) determining the linear refractive index change  $\Delta n$ ,  $I_L(x,y)$  represents the intensity of the graphenelike moiré lattice.  $I_P$  is proportional to  $|\psi(x,y,z)|^2$  determining the nonlinearity of system. We let  $I_P = \gamma|\psi(x,y,z)|^2$ ;  $\gamma = 0$  indicates the lattice system is linear while  $\gamma \neq 0$  indicates the lattice system is nonlinear.

The moiré photonic lattice is a two-dimensional discrete waveguide array with waveguide spacing around 30 microns and the wavelength of the probe beam is 532 nm. Each waveguide in the lattice supports a single bound mode, energy is tightly confined to the waveguides, so the tight-binding approximation is employed, in which only the coupling between the nearest-neighboring waveguides is considered. Hence, the diffraction of light in this discrete model obeys the discrete Schrödinger equation

$$i\partial_z\psi_n(z) = \sum_j c_{nj}\psi_j(z) = \sum_j H_{nj}\psi_j(z), \quad (5)$$

where  $\psi_n$  is the amplitude of the  $n$ th waveguide mode,  $c_{nj}$  is the coupling coefficient between the  $n$ th and  $j$ th waveguide, and  $H$  is the tight-binding Hamiltonian. When the light propagates along the  $z$  direction of the photonic lattice, the propagating modes  $\psi_n$  as a function of  $z$  can be written as  $\psi_n = \psi(x,y)e^{i\beta z}$ . Therefore, there is  $\beta\psi_n = \sum_j c_{nj}\psi_j$ , where

the eigenvalue  $\beta$  plays the role of energy in the analogous Schrödinger equation  $H\psi_n = \beta\psi_n$ . The expression of the coupling mode between the six lattice modes of the graphenelike moiré lattice is

$$\begin{aligned} i\frac{\partial\psi_1(z)}{\partial z} &= c_2[\psi_2(z) + \psi_3(z)] + c_1[\psi_4(z) + \psi_6(z)] \\ i\frac{\partial\psi_2(z)}{\partial z} &= c_2[\psi_1(z) + \psi_3(z)] + c_1[\psi_4(z) + \psi_5(z)] \\ i\frac{\partial\psi_3(z)}{\partial z} &= c_2[\psi_1(z) + \psi_2(z)] + c_1[\psi_5(z) + \psi_6(z)] \\ i\frac{\partial\psi_4(z)}{\partial z} &= c_1[\psi_1(z) + \psi_2(z)] + c_2[\psi_5(z) + \psi_6(z)] \end{aligned}$$

$$\begin{aligned} i\frac{\partial\psi_5(z)}{\partial z} &= c_1[\psi_2(z) + \psi_3(z)] + c_2[\psi_4(z) + \psi_6(z)] \\ i\frac{\partial\psi_6(z)}{\partial z} &= c_1[\psi_1(z) + \psi_3(z)] + c_2[\psi_4(z) + \psi_5(z)], \end{aligned} \quad (6)$$

where  $c_1$  and  $c_2$  are the coupling coefficients of intracell waveguides and intercell waveguides, respectively, as shown in Fig. 1(a). Under the tight-binding approximation, the corresponding Hamiltonian in  $k$  space can be written as

$$H = \begin{pmatrix} 0 & h_{12} & h_{13} & c_1 & 0 & c_1 \\ h_{12}^* & 0 & h_{23} & c_1 & c_1 & 0 \\ h_{13}^* & h_{23}^* & 0 & 0 & c_1 & c_1 \\ c_1 & c_1 & 0 & 0 & h_{45} & h_{46} \\ 0 & c_1 & c_1 & h_{45}^* & 0 & h_{56} \\ c_1 & 0 & c_1 & h_{46}^* & h_{56}^* & 0 \end{pmatrix}, \quad (7)$$

where the variables are  $h_{12} = c_2e^{i(-\frac{\sqrt{3}}{2}k_x - \frac{1}{2}k_y)}$ ,  $h_{13} = c_2e^{i(-k_y)}$ ,  $h_{23} = c_2e^{i(\frac{\sqrt{3}}{2}k_x - \frac{1}{2}k_y)}$ ,  $h_{45} = c_2e^{i(-k_y)}$ ,  $h_{46} = c_2e^{i(\frac{\sqrt{3}}{2}k_x - \frac{1}{2}k_y)}$ ,  $h_{56} = c_2e^{i(\frac{\sqrt{3}}{2}k_x + \frac{1}{2}k_y)}$ ;  $h_{nj}^*$  denotes the complex conjugate of  $h_{nj}$ .

The eigenvalue of the Schrödinger-like equation is called the propagation constant  $\beta$  in paraxial light propagation, and in quantum mechanics is called energy. We calculated the band structure of the infinite graphenelike moiré photonic lattice by solving the eigenvalue  $\beta$  of the Hamiltonian as a function of the Bloch wave vector  $(k_x, k_y)$ . Figure 1(b) presents the band structure of the graphenelike moiré lattice in the tight-binding approximation model. We find that for the bands, there are 12 Dirac cones between band  $\beta_1$  and band  $\beta_2$ , as well as between band  $\beta_4$  and band  $\beta_5$ , which is similar to the Dirac cones in the graphene lattice. Corresponding to the three types of edges in graphene lattice, we truncate the graphenelike moiré lattice to form three edges, namely, the zigzag edge, beard edge, and armchair edge, respectively. The zigzag-edge-type graphenelike moiré lattice is shown in Fig. 1(c), where the zigzag edge is truncated in the  $x$  direction but periodic in the  $y$  direction. The band structure versus  $k_y$  for the moiré lattice with the zigzag edge is calculated and displayed in Fig. 1(d). The black curves in the band structure represent the bulk states, whereas the red curve in the band gap is the edge state. The zigzag edge contains three edge states for a specific incident angle, indicating the edge state is composite. For the other two edges, the band structures show that no edge state is supported, as discussed in Appendix A.

### III. LINEAR EIGENMODES

To further study the characteristics of the zigzag-edge type, we truncate the graphenelike moiré photonic lattice into a triangle with 108 lattice sites whose three edges are all the zigzag-edge type, as depicted in Fig. 2(a). In the experiment, the CW-laser writing technique is employed to establish the finite-sized photonic lattice by light induction of writing waveguides site by site in a 10-mm-long nonlinear photorefractive crystal (SBN), and the results are shown in Fig. 2(b). Here,  $d_1$  and  $d_2$  mark two different lattice spacings between nearest-neighbor lattice sites with values of 35  $\mu\text{m}$  and 32  $\mu\text{m}$ , respectively, which determine the corresponding coupling

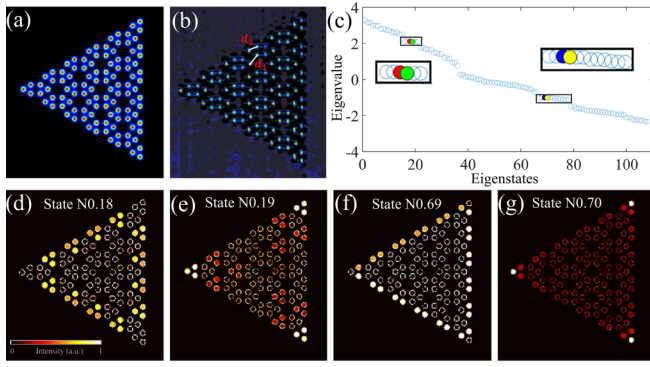


FIG. 2. Truncated graphene-like moiré lattice with the zigzag edge, band structure, mode profiles of the edge states and corner states. (a) Numerically generated discrete models of the triangular graphene-like moiré lattice with the zigzag edge, shown here as a two-dimensional array of waveguides. (b) Experimentally fabricated counterpart of the CW-laser-writing technique. (c), Numerically calculated eigenvalues of the lattice by the tight-binding model. (d)–(g) Mode profiles of four eigenstates localized at the corner [(d), (f)] and edges [(e), (g)] of the lattice, which correspond to states 18 (red dot), 19 (green dot), 69 (blue dot), and 70 (yellow dot) in (c), respectively. The color bar in (d) indicates the normalized intensity of (d)–(g).

coefficients intracell coupling  $c_1$  and intercell coupling  $c_2$  ( $c_1 < c_2$ ), respectively. The experimental setup (the details are in Appendix B) employ a CW plane wave to illuminate spatial light modulator (SLM), then a quasinondiffracting writing beam with variable input position is generated. The photonic lattice remains intact during writing and probing processes due to noninstantaneous photorefractive memory effects. To study the corner states and edge states of the triangular graphene-like moiré photonic lattice, we calculated the energy spectrum. Figure 2(c) shows the ensemble of propagation constants  $\beta$ , which represent the tight-binding eigenvalues of the triangular lattice comprising 108 sites. The colored circles represent two corner states and two edge states. The mode intensity distribution patterns of the four eigenvalues are shown in Figs. 2(d)–2(g). Among them, there exist two types of corner states as illustrated in Figs. 2(e) and 2(g): one of the corner states occupy three corner sites and two nearest-neighbor sites [Fig. 2(e)], one of the other corner states occupy three corner sites [Fig. 2(g)]. Two types of edge states are illustrated in Figs. 2(d) and 2(f), one of the edge states occupy three edges lattice sites and nearest-neighbor sites [Fig. 2(d)] except the sites of corner states as shown in Fig. 2(e), one of the other edge states occupy three edges lattice sites [Fig. 2(f)] except the sites of corner states as shown in Fig. 2(g). Note that when intracell coupling  $c_1$  is greater than intercell coupling  $c_2$ , the mode fields of corner and edge states are almost identical, which are displayed in Appendix C.

#### IV. LINEAR EDGE STATES AND CORNER STATES

To validate the corner and edge states, different probe beams are injected into the lattice. The probe beams diffract discretely due to the coupling between the nearest neighbors and the lattice satisfies the tight-binding approximation model. In the first experiment, the bias electric direct current

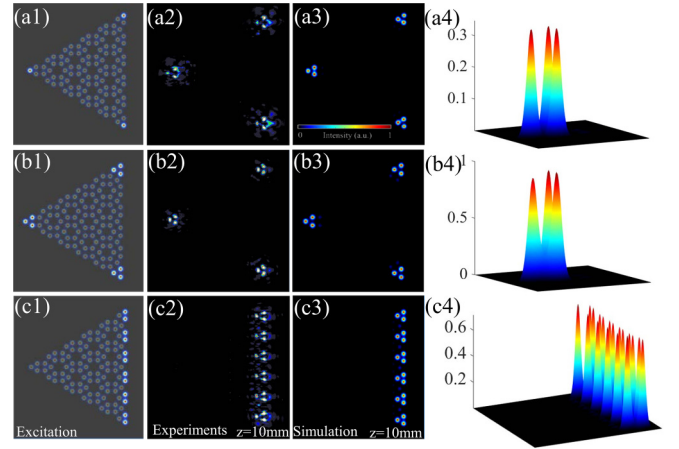


FIG. 3. Experimental demonstration and numerical simulation of linear corner and edge states of the truncated graphene-like moiré lattice. (a1)–(c1) Three excitation patterns of probe beams launched in the lattice: Corner excitations (a1), (b1) and edge excitation (c1). (a2)–(c2) Experimental results for a linear output corresponding to the three initial excitations in (a1)–(c1) after propagation of 10 mm in the lattice. (a3)–(c3) Numerical simulation results corresponding to the same conditions of (a2)–(c2). (a4)–(c4) 3D-view of (a3)–(c3).

field added along the crystalline  $c$  axis of the nonlinear SBN crystal is turned off in the process of probe beam excitation to guarantee the linear property of the moiré lattice. According to the mode distributions of edge states as illustrated in Figs. 2(d)–2(g), we implement three types of excitations as the probe beams that are launched in the lattice: corner excitation [Figs. 3(a1) and 3(b1)] and edge excitation [Fig. 3(c1)]. All the probe beam on excitation sites of the lattice are constituted by Gaussian beams and transverse positions are controlled by the SLM. The distributions of probe beams are represented by the brighter points in Figs. 3(a1)–3(c1). In the first excitation pattern, we excite the three corner sites of the lattice with three single Gaussian probe beams as shown in Fig. 3(a1). After 10-mm propagation in the lattice, the three-vertices single-site excitation leads to discrete diffraction and coupling into the corresponding two nearest waveguides [Fig. 3(a2)]. This experimental result is consistent with edge-state mode profiles of the edge states depicted in Fig. 2(e). For comparison, in a second excitation, the input beams excite on three lattice points at each corner of the lattice [Fig. 3(b1)]. The probe beam remains localized in the excited waveguides after 10-mm propagation; its overall intensity pattern is well maintained [Fig. 3(b2)]. In a third excitation pattern, the input beam excites 12 lattice sites on one side of the lattice. At the end of the SBN crystal, the probe beams are coupled into the nearest lattice sites and no energy is transferred into other waveguides. The experimental results match exactly with the stated lattice sites of the zigzag edge [Fig. 1(c)] and are consistent with edge-state mode profiles depicted in Figs. 2(d) and 2(e). Correspondingly, the numerical simulations on the evolution of a light beam in the linear photonic lattice are performed based on Eq. (4) by the beam propagation method. Numerical simulation results are displayed in Figs. 3(a3)–3(c3) and 3D-view results are in Figs. 3(a4)–3(c4), corresponding to experimental results in Figs. 3(a2)–3(c2), where the simulation propagation

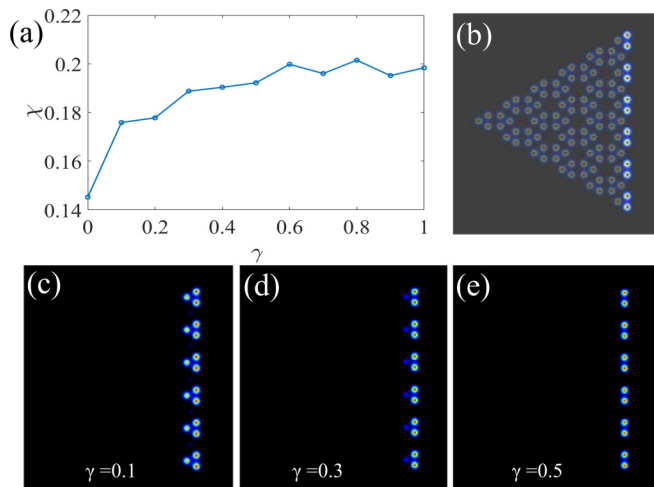


FIG. 4. (a) Form factor of eigenmode of the lattice versus the nonlinearity coefficient  $\gamma$ . (b) The probe beam for excitation of the edge state under nonlinear conditions. (c)–(e), Numerical simulation results at the output plane after 10-mm propagation with  $\gamma = 0.1$ , 0.3, and 0.5, respectively.

distance is 10 mm, corresponding to the length of the SBN crystal used in the experiments. These simulation results agree well with the corresponding experimental results.

## V. NONLINEAR EDGE STATES AND CORNER STATES

Kerr nonlinearity is a widely concerned effect in the photonic lattice, which enables one to balance the diffraction to form spatial solitons. To illustrate the impact of the nonlinear coefficient on the light localization at the edges and corners, we use the integral form factor  $\chi = (\iint |\psi|^4 dx dy)^{1/2} / U$  to characterize the localization strength, where  $U = \iint |\psi|^2 dx dy$  is the energy flow [52]. The dependence of the form factor of the localized mode on nonlinear coefficient  $\gamma$  is shown in Fig. 4(a). With the increase of  $\gamma$ , the value of  $\chi$  is increased, indicating the edge modes become localized gradually. The value of form factor  $\chi$  reaches the maximum when  $\gamma$  reaches 0.6. Similarly, a numerical simulation of the propagation in the nonlinear lattice is launched, and the results are presented in Figs. 4(c)–4(d) for different nonlinearity coefficients  $\gamma$ . Localization gradually increases with the value of  $\gamma$  increasing; the obvious decrease in discrete diffraction marks the onset of nonlinearity effect. When the nonlinearity coefficient reaches  $\gamma=0.5$ , as shown in Fig. 4(e), the probe beam is completely confined to the initially excited waveguides, manifesting a localized edge state.

Lastly, we discuss the numerical and experimental results of edge states and corner states under nonlinear conditions. In the experiment, once the triangular graphenelike moiré lattice is established, the probe beam excitation in the SBN lattice experiences nonlinear propagation when the bias voltage field is turned on. Three excitation patterns as the input beam are also performed under nonlinear condition. In the first excitation pattern, three corner sites are excited [Fig. 5(a1)], the output intensity profile is shown in Fig. 5(a2). The probe beam

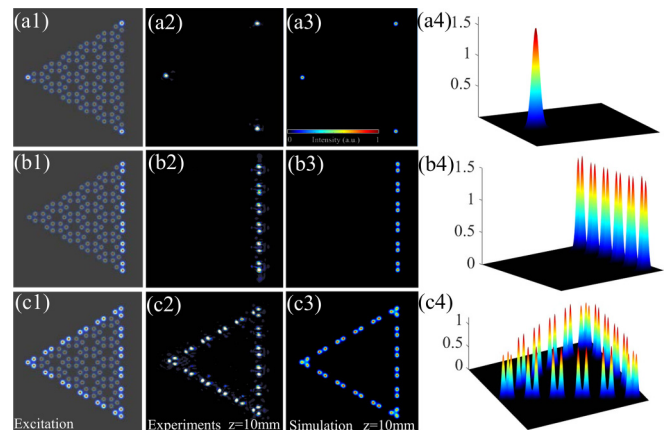


FIG. 5. Experimental demonstration and numerical simulation of nonlinear corner and edge states of the truncated graphenelike moiré lattice. (a1)–(c1) Three excitation patterns of input probe beam launched in lattice under the nonlinear condition. (a2)–(c2) Experimental results for the nonlinear outputs corresponding to different initial excitations sites in (a1)–(c1); after propagating 10 mm in the lattice, the probe beam remains localized in the initially excited lattice sites. (a3)–(c3), Simulation results of transverse intensity pattern of output beam and (a4)–(c4), 3D-view numerical simulation corresponding to the experiments in (a2)–(c2).

is localized in the three corners, and no energy is coupled to other waveguides in comparison with the same excitation pattern for the linear conditions. The result indicates the nonlinearity restricts the light diffraction between waveguides, forming corner localization. In the second and third excitation patterns, the probe beam excites edge states of one edge and three edges, respectively [Figs. 5(b1) and 5(c1)]. These edge states remain intact after 10-mm propagation in the lattice, the output pattern localized, and energy without coupling to other nearest sites [see Figs. 5(b2) and 5(c2)]. We attribute this result to the dynamical balance between diffraction in the lattice and nonlinear self-action, which provide the proper condition for the formation of nonlinear edge states and edge solitons. According to Eq. (4), we perform numerical simulations to examine the nonlinear beam dynamics for the nonlinear excitations. Numerical simulation results [Figs. 5(a3)–5(c3)] and 3D-view numerical simulation [Figs. 5(a4)–5(c4)] output of the probe beam after 10-mm propagation, corresponding to Figs. 5(a2)–5(c2), the probe beam at the output is localized at the excitation sites.

## VI. CONCLUSION

We constructed a graphenelike moiré lattice by superimposing two identical triangular lattices by antiphase and twisting a specific angle. Through calculating the energy bands, they show that the edge state exists only at the zigzag edge. Along with the zigzag edge, the moiré lattice is truncated into a triangular waveguide array with 108 sites. The linear eigenmodes show both the corner and edge states can be supported in such a lattice. Besides, the corner and edge states can also exist when the coupling coefficients between intracell and intercell waveguides are changed, whereafter the high

coincidence of numerical and experimental results verifies the existence of corner and edge states. Further, the optical localization at the edge and corner of the lattice is achieved when nonlinearity is involved. Our research results may bring opportunities to explore intriguing fundamental phenomena such as topology and nonlinear topological solitons in moiré lattices.

### ACKNOWLEDGMENTS

We acknowledge the support of the National Key Research and Development Project of China (Grants No. 2022YFA1404800 and No. 2019YFA0705000), the National Natural Science Foundation of China (Grants No. 12104272, No. 12274270, No. 91950104, No. 12192254, No. 92250304, No. 11974218), and the Local Science and Technology Development Project of the Central Government (Grant No. YDZX20203700001766).

### APPENDIX A: BAND STRUCTURES OF GRAPHENELIKE MOIRÉ LATTICE WITH ARMCHAIR EDGE AND BEARDED EDGE

In this Appendix, the armchair-edge-type moiré lattice structure is periodic in the  $x$  direction and exhibits an armchair edge in the  $y$  direction, as illustrated in Fig. 6(a). The band structure is computed for this moiré lattice with armchair edges and presented in Fig. 6(b) as a function of  $k_x$ . For the bearded edge case, the edge is truncated in the  $x$  direction and the lattice is featured as periodic in the  $y$  direction, as shown in Fig. 6(c). The band structure is calculated and displayed in Fig. 6(d). The results manifest that the bands of the moiré lattice with the two edges exhibit different behaviors of overlapping and degeneracy. However, no edge state is supported by the two edges.

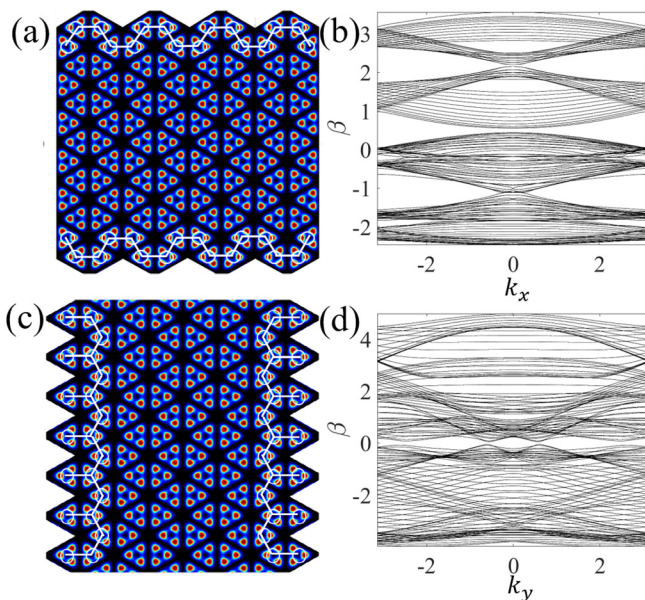


FIG. 6. (a), (b) Schematic image band structure of a graphenelike moiré lattice with an armchair edge. (c), (d) Schematic image band structure of a graphenelike moiré lattice with a bearded edge.

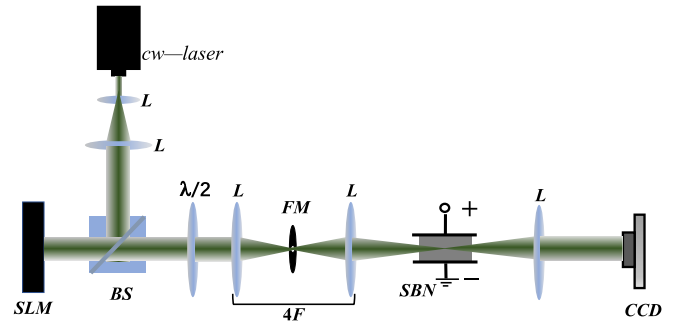


FIG. 7. Experimental setup for site-to-site writing the photonic lattices by a CW laser in a nonlinear photorefractive crystal. SBN: Strontium barium niobate crystal. SLM: Spatial light modulator. BS: Beam splitter. FM: Fourier mask.  $\lambda/2$ : Half-wave plate. L: Optical lens.

### APPENDIX B: EXPERIMENTAL SETUP AND DESCRIPTION

In the experiment, the CW laser-writing technique is employed to write the waveguides site to site by a Gaussian beam as lattice light, enabling the construction of the proposed graphenelike moiré lattice structure. The schematic of experimental setup is shown in Fig. 7. To achieve precise phase modulation of the writing beam, a broad plane beam, generated by a 532 nm laser passing through an objective and focal lens, are used to illuminate a SLM. The designed phase template of a Gaussian beam is uploaded to the SLM, facilitating accurate phase control of the waveguide position. The writing beam, after passing through a half-wave plate, is transformed into ordinary light ( $o$  light) via a  $4f$  system. By adjusting the longitudinal position in the  $z$  direction of the SBN crystal and aligning the crystal center with the waist position of the Gaussian beam, the quas nondiffracting beam can completely pass through the crystal. When a DC bias electric field is applied along the crystalline  $c$  axis of the SBN crystal, the Gaussian beams induce waveguides site to site, leveraging the memory effect of the photorefractive crystal. To simplify the experiment, the probe beam is corouted with the writing beam, reducing the complexity of the setup. In addition, SBN crystals respond differently to changes in the refractive index for ordinary light ( $o$  light) and extraordinary light ( $e$  light). The probe beam is modulated using a half-wave plate to account for this characteristic. The position of each lattice point can be controlled precisely using a SLM which satisfies for constructing the moiré lattice in this paper.

### APPENDIX C: THE MODES OF THE MOIRÉ LATTICE WITH THE ZIGZAG EDGE ( $c_1 > c_2$ AND $c_1 = c_2$ )

In the main text, we discussed the triangular lattice with intracell coupling  $c_1$  being less than intercell coupling  $c_2$  ( $c_1 < c_2$ ). The effect of the ratio of intracell and intercell coupling coefficients on the edge states and corner states is investigated. Here, for comparison, let's consider the energy spectrum of the triangular lattice with zigzag edges when the intracell coupling  $c_1$  is greater than the intercell coupling  $c_2$  ( $c_1 > c_2$ ) [Fig. 8(a)] and when  $c_1$  is equal to  $c_2$  ( $c_1 = c_2$ ) [Fig. 9(a)]. The mode fields of corner and edge states

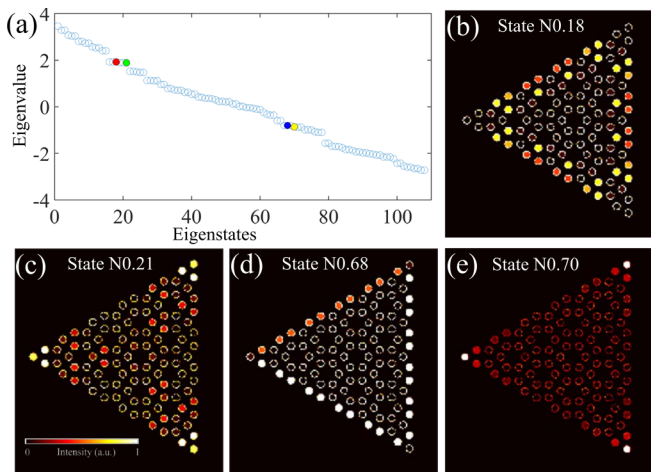


FIG. 8. Triangular graphene-like moiré lattices with zigzag edge, band structure, mode profiles of the edge states and corner states ( $c_1 > c_2$ ). (a) Numerically calculated eigenvalues of the lattice by the tight-binding model, (b)–(e) Mode profiles of four eigenstates localized at the corner and edges of the lattice (states 18, 21, 68, and 70, red, green, blue, and yellow dots, respectively).

corresponding to the numbered locations in the band structure are shown in Figs. 8(b)–8(e) and 9(b)–9(e). There are two types of corner states, as illustrated in Figs. 8(b)–8(e) and 9(b)–9(e), as well as two types of edge states, as depicted

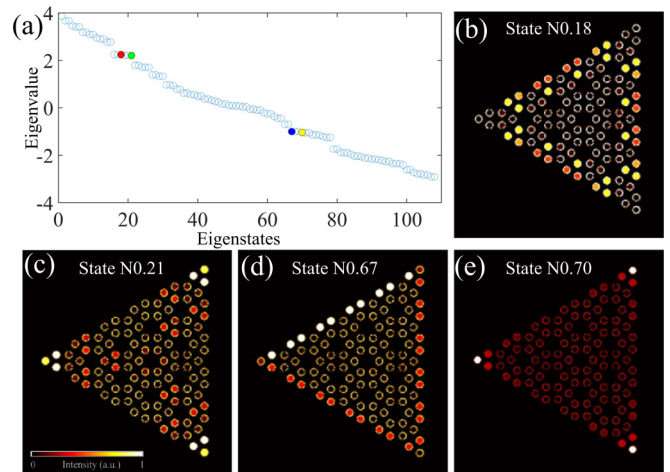


FIG. 9. Triangular graphene-like moiré lattices with zigzag edge, band structure, mode profiles of the edge states and corner states ( $c_1 = c_2$ ). (a) Numerically calculated eigenvalues of the lattice by the tight-binding model, (b)–(e) Mode profiles of four eigenstates localized at the corner and edges of the lattice (states 18, 21, 67 and 70, red, green, blue and yellow dots, respectively).

in Figs. 8(c), 8(e), and 9(b)–9(e). The mode fields of corner and edge states when  $c_1 > c_2$  and  $c_1 = c_2$  are similar to the condition where  $c_1 < c_2$ , except for the state numbers being different.

[1] A. Szameit and S. Nolte, Discrete optics in femtosecond-laser-written photonic structures, *J. Phys. B: At., Mol. Opt. Phys.* **43**, 163001 (2010).

[2] F. Lederer, G. I. Stegeman, D. N. Christodoulides, G. Assanto, M. Segev, and Y. Silberberg, Discrete solitons in optics, *Phys. Rep.* **463**, 1 (2008).

[3] D. Song, V. Paltoglou, S. Liu, Y. Zhu, D. Gallardo, L. Tang, J. Xu, M. Ablowitz, N. K. Efremidis, and Z. Chen, Unveiling pseudospin and angular momentum in photonic graphene, *Nat. Commun.* **6**, 6272 (2015).

[4] D. Song, D. Leykam, J. Su, X. Liu, L. Tang, S. Liu, J. Zhao, N. K. Efremidis, J. Xu, and Z. Chen, Valley Vortex States and Degeneracy Lifting Via Photonic Higher-Band Excitation, *Phys. Rev. Lett.* **122**, 123903 (2019).

[5] X. Liu, S. Xia, E. Jajtić, D. Song, D. Li, L. Tang, D. Leykam, J. Xu, H. Buljan, and Z. Chen, Universal momentum-to-real-space mapping of topological singularities, *Nat. Commun.* **11**, 1586 (2020).

[6] S. Stützer, Y. Plotnik, Y. Lumer, P. Titum, N. H. Lindner, M. Segev, M. C. Rechtsman, and A. Szameit, Photonic topological Anderson insulators, *Nature (London)* **560**, 461 (2018).

[7] M. Segev, Y. Silberberg, and D. N. Christodoulides, Anderson localization of light, *Nat. Photonics* **7**, 197 (2013).

[8] H. Trompeter, W. Krolikowski, D. N. Neshev, A. S. Desyatnikov, A. A. Sukhorukov, Y. S. Kivshar, T. Pertsch, U. Peschel, and F. Lederer, Bloch Oscillations and Zener Tunneling in Two-Dimensional Photonic Lattices, *Phys. Rev. Lett.* **96**, 053903 (2006).

[9] Y. Sun, D. Leykam, S. Nenni, D. Song, H. Chen, Y. D. Chong, and Z. Chen, Observation of Valley Landau-Zener-Bloch Oscillations and Pseudospin Imbalance in Photonic Graphene, *Phys. Rev. Lett.* **121**, 033904 (2018).

[10] S. Mukherjee, A. Spracklen, D. Choudhury, N. Goldman, P. Öhberg, E. Andersson, and R. R. Thomson, Observation of a Localized Flat-Band State in a Photonic Lieb Lattice, *Phys. Rev. Lett.* **114**, 245504 (2015).

[11] R. A. Vicencio, C. Cantillano, L. Morales-Inostroza, B. Real, C. Mejía-Cortés, S. Weimann, A. Szameit, and M. I. Molina, Observation of Localized States in Lieb Photonic Lattices, *Phys. Rev. Lett.* **114**, 245503 (2015).

[12] S. Xia, A. Ramachandran, S. Xia, D. Li, X. Liu, L. Tang, Y. Hu, D. Song, J. Xu, D. Leykam *et al.*, Unconventional Flatband Line States in Photonic Lieb Lattices, *Phys. Rev. Lett.* **121**, 263902 (2018).

[13] L. J. Maczewsky, M. Heinrich, M. Kremer, S. K. Ivanov, M. Ehrhardt, F. Martinez, Y. V. Kartashov, V. V. Konotop, L. Torner, D. Bauer *et al.*, Nonlinearity-induced photonic topological insulator, *Science* **370**, 701 (2020).

[14] Z. Hu, D. Bongiovanni, D. Jukić, E. Jajtić, S. Xia, D. Song, J. Xu, R. Morandotti, H. Buljan, and Z. Chen, Nonlinear control of photonic higher-order topological bound states in the continuum, *Light Sci. Appl.* **10**, 164 (2021).

[15] S. Xia, D. Jukić, N. Wang, D. Smirnova, L. Smirnov, L. Tang, D. Song, A. Szameit, D. Leykam, J. Xu *et al.*, Nontrivial coupling of light into a defect: The interplay of nonlinearity and topology, *Light Sci. Appl.* **9**, 147 (2020).

- [16] R. Fischer, D. Träger, D. N. Neshev, A. A. Sukhorukov, W. Krolikowski, C. Denz, and Y. S. Kivshar, Reduced-Symmetry Two-Dimensional Solitons in Photonic Lattices, *Phys. Rev. Lett.* **96**, 023905 (2006).
- [17] Z. Chen, M. Segev, and D. N. Christodoulides, Optical spatial solitons: Historical overview and recent advances, *Rep. Prog. Phys.* **75**, 086401 (2012).
- [18] S. Mukherjee, A. Spracklen, M. Valiente, E. Andersson, P. Öhberg, N. Goldman, and R. R. Thomson, Experimental observation of anomalous topological edge modes in a slowly driven photonic lattice, *Nat. Commun.* **8**, 13918 (2017).
- [19] S. Mukherjee and M. C. Rechtsman, Observation of Floquet solitons in a topological bandgap, *Science* **368**, 856 (2020).
- [20] Z. Wang, X. Wang, Z. Hu, D. Bongiovanni, D. Jukić, L. Tang, D. Song, R. Morandotti, Z. Chen, and H. Buljan, Sub-symmetry-protected topological states, *Nat. Phys.* **19**, 992 (2023).
- [21] M. Kremer, T. Biesenthal, L. J. Maczewsky, M. Heinrich, R. Thomale, and A. Szameit, Demonstration of a two-dimensional PT-symmetric crystal, *Nat. Commun.* **10**, 435 (2019).
- [22] S. Xia, D. Kaltsas, D. Song, I. Komis, J. Xu, A. Szameit, H. Buljan, K. G. Makris, and Z. Chen, Nonlinear tuning of PT symmetry and non-Hermitian topological states, *Science* **372**, 72 (2021).
- [23] E. Lustig, S. Weimann, Y. Plotnik, Y. Lumer, M. A. Bandres, A. Szameit, and M. Segev, Photonic topological insulator in synthetic dimensions, *Nature (London)* **567**, 356 (2019).
- [24] T. Ozawa, H. M. Price, A. Amo, N. Goldman, M. Hafezi, L. Lu, M. C. Rechtsman, D. Schuster, J. Simon, O. Zilberberg *et al.*, Topological photonics, *Rev. Mod. Phys.* **91**, 015006 (2019).
- [25] Y. Lumer, Y. Plotnik, M. C. Rechtsman, and M. Segev, Self-Localized States in Photonic Topological Insulators, *Phys. Rev. Lett.* **111**, 243905 (2013).
- [26] D. A. Dobrykh, A. V. Yulin, A. P. Slobozhanyuk, A. N. Poddubny, and Y. S. Kivshar, Nonlinear Control of Electromagnetic Topological Edge States, *Phys. Rev. Lett.* **121**, 163901 (2018).
- [27] M. Kohmoto and Y. Hasegawa, Zero modes and edge states of the honeycomb lattice, *Phys. Rev. B* **76**, 205402 (2007).
- [28] M. C. Rechtsman, Y. Plotnik, J. M. Zeuner, D. Song, Z. Chen, A. Szameit, and M. Segev, Topological Creation and Destruction of Edge States in Photonic Graphene, *Phys. Rev. Lett.* **111**, 103901 (2013).
- [29] Y. Plotnik, M. C. Rechtsman, D. Song, M. Heinrich, J. M. Zeuner, S. Nolte, Y. Lumer, N. Malkova, J. Xu, A. Szameit *et al.*, Observation of unconventional edge states in “photonic graphene,” *Nat. Mater.* **13**, 57 (2014).
- [30] M. C. Rechtsman, J. M. Zeuner, Y. Plotnik, Y. Lumer, D. Podolsky, F. Dreisow, S. Nolte, M. Segev, and A. Szameit, Photonic Floquet topological insulators, *Nature (London)* **496**, 196 (2013).
- [31] X. Zhou, Y. Wang, D. Leykam, and Y. D. Chong, Optical isolation with nonlinear topological photonics, *New J. Phys.* **19**, 095002 (2017).
- [32] Y. V. Kartashov and D. V. Skryabin, Bistable Topological Insulator with Exciton-Polaritons, *Phys. Rev. Lett.* **119**, 253904 (2017).
- [33] Z. Yang, E. Lustig, Y. Lumer, and M. Segev, Photonic Floquet topological insulators in a fractal lattice, *Light Sci. Appl.* **9**, 128 (2020).
- [34] M. S. Kirsch, Y. Zhang, M. Kremer, L. J. Maczewsky, S. K. Ivanov, Y. V. Kartashov, L. Torner, D. Bauer, A. Szameit, and M. Heinrich, Nonlinear second-order photonic topological insulators, *Nat. Phys.* **17**, 995 (2021).
- [35] F. Zangeneh-Nejad and R. Fleury, Nonlinear Second-Order Topological Insulators, *Phys. Rev. Lett.* **123**, 053902 (2019).
- [36] Z. Zhang, R. Wang, Y. Zhang, Y. V. Kartashov, F. Li, H. Zhong, H. Guan, K. Gao, F. Li, Y. Zhang *et al.*, Observation of edge solitons in photonic graphene, *Nat. Commun.* **11**, 1902 (2020).
- [37] D. Leykam and Y. D. Chong, Edge Solitons in Nonlinear-Photonic Topological Insulators, *Phys. Rev. Lett.* **117**, 143901 (2016).
- [38] R. Decker, Y. Wang, V. W. Brar, W. Regan, H.-Z. Tsai, Q. Wu, W. Gannett, A. Zettl, and M. F. Crommie, Local electronic properties of graphene on a Bn substrate via scanning tunneling microscopy, *Nano Lett.* **11**, 2291 (2011).
- [39] C. Woods, L. Britnell, A. Eckmann, R. Ma, J. Lu, H. Guo, X. Lin, G. Yu, Y. Cao, R. V. Gorbachev *et al.*, Commensurate-incommensurate transition in graphene on hexagonal boron nitride, *Nat. Phys.* **10**, 451 (2014).
- [40] Y. Cao, V. Fatemi, A. Demir, S. Fang, S. L. Tomarken, J. Y. Luo, J. D. Sanchez-Yamagishi, K. Watanabe, T. Taniguchi, E. Kaxiras *et al.*, Correlated insulator behaviour at half-filling in magic-angle graphene superlattices, *Nature (London)* **556**, 80 (2018).
- [41] Y. Cao, V. Fatemi, S. Fang, K. Watanabe, T. Taniguchi, E. Kaxiras, and P. Jarillo-Herrero, Unconventional superconductivity in magic-angle graphene superlattices, *Nature (London)* **556**, 43 (2018).
- [42] S. J. Ahn, P. Moon, T.-H. Kim, H.-W. Kim, H.-C. Shin, E. H. Kim, H. W. Cha, S.-J. Kahng, P. Kim, M. Koshino *et al.*, Dirac electrons in a dodecagonal graphene quasicrystal, *Science* **361**, 782 (2018).
- [43] R. Bistritzer and A. H. MacDonald, Moiré bands in twisted double-layer graphene, *Proc. Natl. Acad. Sci. USA* **108**, 12233 (2011).
- [44] S. Carr, D. Massatt, S. Fang, P. Cazeaux, M. Luskin, and E. Kaxiras, Twistronics: Manipulating the electronic properties of two-dimensional layered structures through their twist angle, *Phys. Rev. B* **95**, 075420 (2017).
- [45] C. R. Dean, L. Wang, P. Maher, C. Forsythe, F. Ghahari, Y. Gao, J. Katoch, M. Ishigami, P. Moon, M. Koshino *et al.*, Hofstadter’s butterfly and the fractal quantum Hall effect in moiré superlattices, *Nature (London)* **497**, 598 (2013).
- [46] M. Koshino, Band structure and topological properties of twisted double bilayer graphene, *Phys. Rev. B* **99**, 235406 (2019).
- [47] Y. Wang, J. Herzog-Arbeitman, G. W. Burg, J. Zhu, K. Watanabe, T. Taniguchi, A. H. MacDonald, B. A. Bernevig, and E. Tutuc, Bulk and edge properties of twisted double bilayer graphene, *Nat. Phys.* **18**, 48 (2022).
- [48] A. González-Tudela and J. I. Cirac, Cold atoms in twisted-bilayer optical potentials, *Phys. Rev. A* **100**, 053604 (2019).
- [49] T. Salamon, A. Celi, R. W. Chhajlany, I. Frérot, M. Lewenstein, L. Tarruell, and D. Rakshit, Simulating Twistronics without a Twist, *Phys. Rev. Lett.* **125**, 030504 (2020).



- [50] P. San-Jose, J. González, and F. Guinea, Non-Abelian Gauge Potentials in Graphene Bilayers, *Phys. Rev. Lett.* **108**, 216802 (2012).
- [51] L. J. O’Riordan, A. C. White, and T. Busch, Moiré superlattice structures in kicked Bose-Einstein condensates, *Phys. Rev. A* **93**, 023609 (2016).
- [52] P. Wang, Y. Zheng, X. Chen, C. Huang, Y. V. Kartashov, L. Torner, V. V. Konotop, and F. Ye, Localization and delocalization of light in photonic moiré lattices, *Nature (London)* **577**, 42 (2020).
- [53] Q. Fu, P. Wang, C. Huang, Y. V. Kartashov, L. Torner, V. V. Konotop, and F. Ye, Optical soliton formation controlled by angle twisting in photonic moiré lattices, *Nat. Photonics* **14**, 663 (2020).
- [54] Y. V. Kartashov, F. Ye, V. V. Konotop, and L. Torner, Multifrequency Solitons in Commensurate-Incommensurate Photonic Moiré Lattices, *Phys. Rev. Lett.* **127**, 163902 (2021).
- [55] A. A. Arkhipova, Y. V. Kartashov, S. K. Ivanov, S. A. Zhuravitskii, N. N. Skryabin, I. V. Dyakonov, A. A. Kalinkin, S. P. Kulik, V. O. Kompanets, S. V. Chekalin, F. Ye, V. V. Konotop, L. Torner, and V. N. Zadkov, Observation of Linear and Nonlinear Light Localization at the Edges of Moiré Lattices, *Phys. Rev. Lett.* **130**, 083801 (2023).
- [56] C. Shang, C. Lu, S. Tang, Y. Gao, and Z. Wen, Generation of gradient photonic moiré lattice fields, *Opt. Express* **29**, 29116 (2021).